

UNIVERSITY *of* York

This is a repository copy of *Lytic xylan oxidases from wood-decay fungi unlock biomass degradation*.

White Rose Research Online URL for this paper:
<https://eprints.whiterose.ac.uk/126886/>

Version: Accepted Version

Article:

Couturier, Marie, Ladevèze, Simon, Sulzenbacher, Gerlind et al. (19 more authors) (2018) Lytic xylan oxidases from wood-decay fungi unlock biomass degradation. NATURE CHEMICAL BIOLOGY. pp. 306-310. ISSN 1552-4450

<https://doi.org/10.1038/nchembio.2558>

Reuse

Items deposited in White Rose Research Online are protected by copyright, with all rights reserved unless indicated otherwise. They may be downloaded and/or printed for private study, or other acts as permitted by national copyright laws. The publisher or other rights holders may allow further reproduction and re-use of the full text version. This is indicated by the licence information on the White Rose Research Online record for the item.

Takedown

If you consider content in White Rose Research Online to be in breach of UK law, please notify us by emailing eprints@whiterose.ac.uk including the URL of the record and the reason for the withdrawal request.



eprints@whiterose.ac.uk
<https://eprints.whiterose.ac.uk/>

1 **Lytic xylan oxidases from wood-decay fungi unlock biomass degradation**

2 Marie Couturier^{1,*}, Simon Ladevèze^{1,*}, Gerlind Sulzenbacher^{2,3}, Luisa Ciano⁴, Mathieu Fanuel⁵,
3 Céline Moreau⁵, Ana Villares⁵, Bernard Cathala⁵, Florence Chaspoul⁶, Kristian E. Frandsen¹,
4 Aurore Labourel¹, Isabelle Herpoël-Gimbert¹, Sacha Grisel¹, Mireille Haon¹, Nicolas Lenfant²,
5 Hélène Rogniaux⁵, David Ropartz⁵, Gideon Davies⁴, Marie-Noëlle Rosso¹, Paul H. Walton⁴,
6 Bernard Henrissat^{2,3,7}, Jean-Guy Berrin^{1,**}

7 ¹INRA, Aix Marseille Univ., Biodiversité et Biotechnologie Fongiques (BBF), UMR1163, F-
8 13009 Marseille, France

9 ²Architecture et Fonction des Macromolécules Biologiques (AFMB), CNRS, Aix-Marseille
10 Univ., F-13009 Marseille, France

11 ³INRA, USC1408 Architecture et Fonction des Macromolécules Biologiques (AFMB), F-13009
12 Marseille, France

13 ⁴Department of Chemistry, University of York, York, UK, YO10 5DD

14 ⁵INRA, Unité de Recherche Biopolymères Interactions Assemblages (BIA), F-44316 Nantes,
15 France

16 ⁶IMBE Aix Marseille Univ., IRD CNRS UAPV, Faculté de Pharmacie, F-13005 Marseille,
17 France.

18 ⁷Department of Biological Sciences, King Abdulaziz University, Jeddah, Saudi Arabia

19 *These authors contributed equally to this work

20 **Correspondence and request to materials should be addressed to J.G.B.

21 (jean-guy.berrin@inra.fr)

22

23 **Abstract**

24 Wood biomass is the most abundant feedstock envisioned for the development of modern
25 biorefineries. However, the cost-effective conversion of this form of biomass to commodity
26 products is limited by its resistance to enzymatic degradation. Here we describe a new family of
27 fungal lytic polysaccharide monooxygenases (LPMOs) prevalent amongst white-rot and brown-
28 rot basidiomycetes, which is active on xylans - a recalcitrant polysaccharide abundant in wood
29 biomass. Two AA14 LPMO members from the white-rot fungus *Pycnoporus coccineus*
30 significantly increase the efficiency of wood saccharification through oxidative cleavage of
31 highly refractory xylan-coated cellulose fibers. The discovery of this unique enzyme activity
32 advances our knowledge on the degradation of woody biomass in nature and offers an innovative
33 solution to improve enzyme cocktails for biorefinery applications.

34

35

36 **Introduction**

37 Wood is the most abundant organic source of biomass on Earth, with an annual production of
38 about 5.64×10^{10} tons of carbon¹. Its widespread nature has allowed humans to use it in many
39 contexts, most notably as a building material due to its exceptional mechanical properties and
40 resistance to decay. In bio-based industries, the utilization of wood is taking on a new
41 importance as it constitutes the most promising source for advanced biofuels and plant-derived
42 products. Notwithstanding its potential, however, the cost-effective conversion of woody
43 feedstocks is limited by a single key factor, the recalcitrance of the lignocellulosic matrix to
44 degradation by enzyme cocktails². To overcome this recalcitrance, biorefineries utilize energy-
45 demanding pretreatment processes to solubilize the inaccessible biomass components before
46 enzymatic saccharification. The recalcitrant fraction reflects its heteroxylan content which is
47 known to be particularly resistant to xylanases due to extensive decoration and because these
48 xylans can adopt a flat conformation with their chains solidly adhering *via* hydrogen-bonds to the
49 surface of cellulose microfibrils^{3,4}. Finding sustainable means of overcoming this resistance to
50 degradation is one of the main challenges faced by modern biorefineries. Indeed, the xylan
51 problem is so severe that consideration is being given to engineering energy crops modified to
52 contain fewer recalcitrant xylans⁵.

53 In nature, fungi play a vital role in the terrestrial carbon cycle and dominate wood decomposition
54 in boreal forests⁶. Wood-decaying basidiomycetes classified as white-rot and brown-rot fungi,
55 naturally degrade cellulose and hemicelluloses using a large diversity of carbohydrate-active
56 enzymes (CAZymes; www.cazy.org)⁷ and Fenton-type chemistry⁸. In this context, understanding
57 of plant-cell wall deconstruction was recently overturned by the discovery of lytic
58 polysaccharide monooxygenases (LPMOs) enzymes which cleave polysaccharides through an

59 oxidative as opposed to hydrolytic mechanism⁹⁻¹¹. Such is their importance, that industrial
60 enzyme mixtures for the conversion of agricultural residues to biofuels now incorporate
61 cellulose-active LPMOs¹², helping biorefineries move towards environmental and economic
62 sustainability. Despite the significant efficiencies that LPMOs have brought to biomass
63 degradation, industrial enzyme cocktails are still unable to degrade woody biomass completely
64 and there is a major need to identify new enzymes capable of effecting this breakdown. From
65 this perspective, there are three fungal LPMO families (termed AA9, AA11 and AA13 in the
66 CAZy classification)⁷, which were discovered from genome sequences by virtue of their modular
67 structure where the catalytic LPMO domain is sometimes appended to known substrate-targeting
68 carbohydrate-binding modules (CBMs). Each fungal LPMO family is associated with the
69 oxidative cleavage of distinct polysaccharides with AA9 acting mainly on cellulose and
70 xyloglucan¹⁰, AA11 on chitin¹³ and AA13 on starch^{14,15}; a solely xylan-acting LPMO is
71 conspicuous by its absence.

72 Using comparative post-genomic approaches among fungal wood decayers, we identified the
73 existence of a previously unknown family of LPMO. This new family to be termed AA14 in the
74 CAZy classification differs phylogenetically and structurally from the previous AA9, AA10,
75 AA11 and AA13 families. The first characterized members from the white-rot basidiomycete
76 fungus *Pycnoporus coccineus* target xylan chains covering wood cellulose fibers thus unlocking
77 the enzymatic degradation of wood biomass.

78 **Results**

79 **Discovery of the AA14 family among fungal wood decayers**

80 The white-rot basidiomycete *Pycnoporus coccineus* is an efficient degrader of both hardwood
81 and softwood¹⁶. While studying the effect of different types of biomass on *P. coccineus* growth
82 using transcriptomics and secretomics, we identified a gene encoding a protein of unknown
83 function that was highly up-regulated on pine and poplar as compared to control¹⁶. The
84 corresponding protein (JGI ID 1372210; GenBank ID #KY769370) was secreted only during
85 growth on pine and poplar suggesting a role in wood decay. A BLAST search against public
86 sequence databases identified more than 300 proteins with significant similarity to #KY769370
87 from *P. coccineus*, many of which from well-known saprotrophic fungi. Sequence alignment
88 revealed a conserved N-terminal histidine (**Supplementary Fig. 1**), commensurate with a
89 copper-binding histidine brace active site¹⁰, which is a hallmark of known LPMOs. A
90 phylogenetic analysis shows that the newly identified sequences strongly cluster together with
91 high bootstrap values and are very distant from AA9, AA10, AA11 and AA13 sequences
92 (**Supplementary Fig. 2**), thereby defining a new LPMO family designated AA14 in the CAZy
93 database. AA14 members are found in all well-known white-rot (*Pleurotus ostreatus*,
94 *Phanerochaete chrysosporium*, *Trametes versicolor*) and brown-rot (*Serpula lacrymans*,
95 *Coniophora puteana*, *Postia placenta*) basidiomycetes and in some wood-inhabitants
96 ascomycetes within the *Xylariaceae* and *Hypocreaceae* families. A slight gene family expansion
97 is observed in wood-decaying basidiomycetes (average number per species 3.35 in
98 basidiomycetes and 1.28 in ascomycetes) (**Fig. 1; Supplementary Data Set 1**). None of the
99 AA14 members identified in fungal genomes harbors a carbohydrate-binding module (CBM)

100 explaining why this family was not previously discovered together with AA11 and AA13
101 through the “module walk” approach^{13,15}.

102 **Expression and biochemical characterization of *PcAA14***

103 Two *P. coccineus* proteins, *PcAA14A* (#KY769369) and *PcAA14B* (#KY769370), displaying
104 65% sequence identity were produced to high yield in *Pichia pastoris*, purified to homogeneity
105 and biochemically characterized (**Supplementary Table 1; Supplementary Fig. 3 and 4**). We
106 confirmed the correct processing of the native signal peptide, which exposed the N-terminal
107 histidine residue at position 1 in the mature polypeptide chain (**Supplementary Table 1**). Mass
108 spectrometry analyses revealed that both proteins contained ~ one copper atom per protein
109 molecule and treatment with EDTA led to partial apo forms (~0.1 copper atom per protein
110 molecule). *PcAA14A* and *PcAA14B* were both able to produce hydrogen peroxide in the
111 presence of ascorbate, cysteine or gallate as electron donors (**Supplementary Table 2**).

112 **Crystal structure of *PcAA14***

113 The structure of *PcAA14B* was solved by multiple-wavelength anomalous dispersion data
114 recorded at the gadolinium edge, and refined at 3.0 Å resolution. The core of the protein folds
115 into a largely antiparallel immunoglobulin-like β-sandwich (**Fig. 2a**), a fold globally similar to
116 that seen in LPMOs from other families. The active site of *PcAA14B* constituted by His1, His99
117 and Tyr176 forming the canonical histidine brace is exposed at the surface (**Fig. 2b**). In contrast
118 to the flat substrate-binding surfaces observed in AA9 LPMOs¹⁷, the *PcAA14B* surface has a
119 rippled shape with a clamp formed by two prominent surface loops (**Supplementary Fig. 5**).
120 Both loops are located in the N-terminal half of *PcAA14B*, and are equivalent to the L2 and L3
121 loop regions in AA9 LPMOs. Conventionally, the N-terminal part of AA9 LPMOs upstream of
122 the L2 loop region makes up a β-strand segment (single β-strand or a β-hairpin). No equivalent

123 β -strands are found in the *PcAA14B* structure, which, in contrast, forms loop segments
124 immediately after the N-terminal His (**Supplementary Fig. 5**). The *PcAA14B* structure also
125 reveals a cystine (Cys67-Cys90) in the L3-equivalent region, which borders an extension not
126 present in AA9 LPMOs (**Supplementary Fig. 5**). It is highly interesting to note that the two
127 loops making up the clamp in *PcAA14B* correspond to modified L2 and L3 loop regions, as
128 these have been shown to be involved in LPMO-substrate interactions¹⁷. For AA9 LPMOs a
129 conserved Tyr has been shown to be involved in substrate interactions at the active site surface¹⁷.
130 Interestingly, *PcAA14B* possesses equally a conserved tyrosine residue at the edge of the
131 substrate-binding surface, Tyr240, albeit located on a different loop region, which could
132 potentially make substrate interactions. Overall the crystal structure of *PcAA14B* reveals novel
133 features within its putative substrate binding site, which may suggest differences in terms of
134 substrate specificity compared to known LPMOs.

135 **EPR spectroscopic analysis of the copper site of *PcAA14***

136 Multi-frequency Electron Paramagnetic Resonance (EPR) analysis was carried out on both
137 *PcAA14A* and *PcAA14B* to determine the nature of the copper active site (Figure 2C;
138 **Supplementary Fig. 6**). The spin Hamiltonian parameters (**Supplementary Table 3**) displayed
139 axial parameters ($g_x \approx g_y < g_z$) with a $d(x^2-y^2)$ SOMO, placing the copper active site squarely
140 within a type 2 Peisach-Blumberg classification¹⁸. Simulations required the addition of two ($I=1$)
141 nitrogen atoms (coupling in the range of 30 to 36 MHz), as would be expected from the
142 coordinating histidine side chains. Overall, these spin-Hamiltonian parameters are similar to
143 those obtained for AA9 LPMOs confirming the presence of the copper(II) ion within the
144 histidine brace coordination environment¹⁹. These data support the hypothesis that *PcAA14s*
145 display LPMO characteristics and that copper is their native metal cofactor.

146 **Substrate specificity of PcAA14**

147 Activity assays were initially carried out with PcAA14A and PcAA14B on a wide range of
148 polysaccharides including cellulose and xylans in the presence of ascorbic acid, which is widely
149 used as electron donor for LPMOs. Using standardized methods previously employed to
150 characterize AA9 LPMOs²⁰, no activity could be detected on these polysaccharides. Next, we
151 performed saccharification assays on pretreated biomass including poplar, pine and wheat straw
152 using a *Trichoderma reesei* CL847 cocktail mainly composed of cellulases and xylanases²¹. A
153 boost of glucose release from poplar and pine was observed upon addition of either of the AA14
154 enzymes to the cocktail (**Fig. 3a**). When the reactions were conducted in absence of a reductant
155 the boost effect was maintained (**Supplementary Fig. 8**), suggesting that one of the components
156 from the biomass (e.g. lignin) may act as an electron donor²². This improvement in glucose
157 release was dose-dependent yielding up to ~100% increase on pretreated softwood (**Fig. 3b**).
158 However, no significant boost was observed on wheat straw (**Supplementary Fig. 8**), which
159 differs in terms of hemicellulose composition compared to wood, indicating that AA14 enzymes
160 specifically target one of the components of woody biomass. In a finding with important
161 consequences for biorefinery use of woody biomass as feedstock, the *T. reesei* CL847 cocktail
162 enriched in AA9 LPMO acting on cellulose was also boosted by PcAA14A, suggesting that AA9
163 and AA14 enzymes may act on different regions within the lignocellulosic matrix
164 (**Supplementary Fig. 8**). Because AA14 members do not harbor any CBM module, we
165 artificially attached a fungal CBM1 module targeting crystalline cellulose to PcAA14A. The
166 resulting modular PcAA14A-CBM1 enzyme performed less efficiently than the catalytic module
167 alone (**Supplementary Fig. 8**), suggesting that AA14 enzymes may not require specific binding
168 to the flat crystalline cellulose surface.

169 To discern which polymer was attacked by AA14 enzymes, we used birchwood cellulosic fibers,
170 consisting of 79% cellulose and 21% xylan, as a substrate. After incubation with *PcAA14A* or
171 *PcAA14B*, wood fibers were disrupted (**Fig. 4a**) uncovering cellulose structures visualized at
172 different scales using transmission electron microscopy and atomic force microscopy
173 (**Supplementary Fig. 9**). These observations suggest a weakening of the cohesive forces that
174 link the wood fibers together in a manner similar to that previously described with AA9
175 enzymes²³. Samples treated with AA14 enzymes were further analyzed using solid-state Cross-
176 Polarization Magic Angle Spinning ¹³C Nuclear Magnetic Resonance (¹³C CP/MAS NMR). The
177 impact of AA14 enzymes on the fibers was different to that recently observed for AA9
178 LPMOs²³. In the case of *PcAA14* enzymes, no meaningful change was observed on cellulose
179 signals (**Fig. 4b**; **Supplementary Fig. 10**). Interestingly, however, significant changes in signal
180 areas corresponding to hemicelluloses located at 101 ppm and 82 ppm were observed when the
181 NMR spectra were deconvoluted in the C-1 and the C-4 regions (**Supplementary Fig. 10**).
182 These results suggest that AA14 enzymes act on xylans bound to cellulose, which have a rigidity
183 and a conformation similar to that of the underlying cellulose chains⁴. The specific attack of
184 *PcAA14* on xylan substrates differentiates this new class of enzymes from all other LPMOs^{24,25},
185 none of which has previously been reported to oxidize xylan in such a selective and efficient
186 manner.

187 To further substantiate the idea that AA14 enzymes act on xylan bound to cellulose, we
188 performed synergy assays of AA14 enzymes in combination with a fungal GH11 xylanase using
189 birchwood cellulosic fibers. Addition of *PcAA14A* to a GH11 xylanase significantly increased
190 by 40% the release of xylo-oligomers from birchwood cellulosic fibers (Figure 4C;
191 **Supplementary Fig. 11**). Additionally, no improvement of xylan conversion was observed on

192 birchwood cellulosic fibers when the xylanase was combined with a cellulose-acting AA9
193 LPMO (**Fig. 4c**).

194 We further investigated the nature of soluble products generated after synergistic action of
195 *PcAA14A* and the GH11 xylanase. Using ionic chromatography, a range of oligosaccharides
196 eluted at similar retention time to C1-oxidized oligosaccharides (**Supplementary Fig. 11**). Mass
197 spectrometry analyses performed on the same samples allowed the identification of several
198 putative oxidative species with masses corresponding to C1-oxidized xylotriose (X3ox) and C1-
199 oxidized xylo-tetraose (X4ox) and non-oxidized xylo-oligosaccharides substituted with
200 glucuronic acid (X₃MeGlcA, X₄MeGlcA, X₅MeGlcA) (**Supplementary Fig. 12**). The structure
201 of the C1-oxidized xylotriose with an aldonic acid on the reducing end (**Fig. 4d**) was confirmed
202 by fragmentation of the species observed at 429 *m/z* by tandem MS (MS/MS) (**Supplementary**
203 **Fig. 12**). The identification of oxidative products demonstrates that AA14 enzymes are LPMOs.
204

205 Discussion

206 Our findings that xylans are susceptible to AA14 oxidative cleavage only when adsorbed onto
207 crystalline cellulose and not when in solution are supported by reports that showed that xylans
208 exist in different contexts within the cell wall^{4,26}. Recalcitrant xylans bound to cellulose
209 microfibrils display a two-fold screw axis conformation aligned parallel to the cellulose chain
210 direction⁴ that is compatible with the proper orientation of the carbohydrate H1 and H4 atoms
211 with respect to the LPMO catalytic center²². Unravelling the substrate specificity of AA14s has
212 been challenging as these enzymes are not active on xylans in solution most probably due to the
213 three-fold helical screw conformation of the substrate²⁷. Using multidisciplinary approaches, we
214 reveal that AA14 LPMOs probably target specifically the protective shield made by heteroxylans

215 that cover cellulose microfibrils in wood. The conformation of xylan in this context contributes
216 to wood recalcitrance and glycoside hydrolases are not able to access such a sterically restricted
217 substrate. The cleavage of these rare motifs by AA14 LPMOs unlocks the accessibility of xylan
218 and cellulose chains to glycoside hydrolases therefore improving the overall saccharification of
219 woody biomass. These results not only greatly enhance our knowledge of wood superstructure,
220 they also contribute to understand and better exploit biomass deconstruction by fungal
221 saprotrophs.

222

223 **Acknowledgements.** We thank the European Synchrotron Radiation Facility (Grenoble), and the
224 synchrotron Soleil (Gif-sur-Yvette) for beam time allocation and assistance. We thank S. Tapin
225 for providing cellulose fibers, E. Bonnin and J. Vigouroux for compositional analyses, G. Toriz
226 and P. Gatenholm for providing purified wood xylan, L. Foucat and X. Falourd for their valued
227 assistance with treatments of the NMR data, E. Perrin for the excellent technical support for
228 TEM images, B. Seantier for the access and assistance to AFM facilities, D. Hartmann and E.
229 Bertrand for their help with enzyme production in bioreactor, and D. Navarro and G. Anasontzis
230 for insightful discussions. MC was funded by a Marie Curie International Outgoing Fellowship
231 within the 7th European Community Framework Program (328162). SL, MNR and JGB were
232 funded by the Microbio-E A*MIDEX project (ANR-11-IDEX-0001-02). This work was
233 supported in part by the CNRS and the French Infrastructure for Integrated Structural Biology
234 (FRISBI) ANR-10-INSB-05-01. NL and BH were supported by Agence Française de
235 l'Environnement et de la Maîtrise de l'Energie (1201C102). PHW, GJD and LC thank the UK
236 Biotechnology and Biological Sciences Research Council (BB/L001926/1 and BB/L021633/1)
237 for funding. GJD is the Royal Society Ken Murray Research Professor.

238 **Author contributions.** MC and SL contributed equally to this work. MC identified the new
239 enzymes and performed biochemical characterization. MNR was in charge of transcriptomic and
240 proteomic analyses. MC, SL, SG, IG and MH performed production of proteins in flasks and
241 bioreactors. FC performed ICP-MS analysis. SL and SG performed synergy assays with xylanase
242 and protein crystallization. SL and GS solved the crystal structure. BH and NL performed
243 bioinformatic analyses. MC, SL, SG performed HPAEC analyses. MF, DR and HR identified
244 oxidized products using mass spectrometry. MC, SG and IG performed saccharification assays.
245 AV, CM and BC carried out microscopy and NMR analyses. LC performed the EPR study under
246 the direction of PHW and GJD. JGB supervised the work and organized the data. The manuscript
247 was written by JGB with contributions from BH and PHW. All authors made comments on the
248 manuscript and approved the final version. Figures were prepared by JGB, KEF, AL, NL, SL,
249 LC, MF, SG and IG.

250 **Competing Financial Interests Statement.** The authors declare no competing financial
251 interests.

252

253

254 **References**

- 255 1. Field, C. B., Behrenfeld, M. J., Randerson, J. T. & Falkowski, P. Primary production of the
256 biosphere: integrating terrestrial and oceanic components. *Science* **281**, 237-240 (1998)
- 257 2. Himmel, M. E. *et al.* Biomass recalcitrance: engineering plants and enzymes for biofuels production.
258 *Science* **315**, 804-807 (2007)
- 259 3. Biely, P., Singh, S. & Puchart, V. Towards enzymatic breakdown of complex plant xylan structures:
260 State of the art. *Biotechnol. Adv.* **34**, 1260-1274 (2016)
- 261 4. Simmons, T. J. *et al.* Folding of xylan onto cellulose fibrils in plant cell walls revealed by solid-state
262 NMR. *Nat. Commun.* **7**, 13902 (2016)
- 263 5. Loqué, D., Scheller, H. V. & Pauly, M. Engineering of plant cell walls for enhanced biofuel
264 production. *Curr. Opin. Plant Biol.* **25**, 151-161 (2015)
- 265 6. Hibbett, D. S. & Donoghue, M. J. Analysis of character correlations among wood decay
266 mechanisms, mating systems, and substrate ranges in homobasidiomycetes. *Syst. Biol.* **50**, 215-242
267 (2001)
- 268 7. Lombard, V., Golaconda Ramulu, H., Drula, E., Coutinho, P. M. & Henrissat, B. The carbohydrate-
269 active enzymes database (CAZy) in 2013. *Nucleic Acids Res.* **42**, D490-495 (2014)
- 270 8. Riley, R. *et al.* Extensive sampling of basidiomycete genomes demonstrates inadequacy of the white-
271 rot/brown-rot paradigm for wood decay fungi. *Proc. Natl. Acad. Sci. U.S.A.* **111**, 9923-9928 (2014)
- 272 9. Vaaje-Kolstad, G. *et al.* An oxidative enzyme boosting the enzymatic conversion of recalcitrant
273 polysaccharides. *Science* **330**, 219-222 (2010)
- 274 10. Quinlan, R. J. *et al.* Insights into the oxidative degradation of cellulose by a copper metalloenzyme
275 that exploits biomass components. *Proc. Natl. Acad. Sci. U.S.A.* **108**, 15079-15084 (2011)
- 276 11. Kracher, D. *et al.* Extracellular electron transfer systems fuel cellulose oxidative degradation.
277 *Science* **352**, 1098-1101 (2016)

- 278 12. Johansen, K. S. Discovery and industrial applications of lytic polysaccharide mono-oxygenases.
279 *Biochem. Soc. Trans.* **44**, 143-149 (2016)
- 280 13. Hemsworth, G. R., Henrissat, B., Davies, G. J. & Walton, P. H. Discovery and characterization of a
281 new family of lytic polysaccharide monooxygenases. *Nat. Chem. Biol.* **10**, 122-126 (2014)
- 282 14. Vu, V. V., Beeson, W. T., Span, E. A., Farquhar, E. R. & Marletta, M. A. A family of starch-active
283 polysaccharide monooxygenases. *Proc. Natl. Acad. Sci. U.S.A.* **111**, 13822-13827 (2014)
- 284 15. Lo Leggio, L. *et al.* Structure and boosting activity of a starch-degrading lytic polysaccharide
285 monooxygenase. *Nat. Commun.* **6**, 5961 (2015)
- 286 16. Couturier, M. *et al.* Enhanced degradation of softwood versus hardwood by the white-rot fungus
287 *Pycnoporus coccineus*. *Biotechnol. Biofuels* **8**, 216 (2015)
- 288 17. Frandsen, K. E. *et al.* The molecular basis of polysaccharide cleavage by lytic polysaccharide
289 monooxygenases. *Nat. Chem. Biol.* **12**, 298-303 (2016)
- 290 18. Peisach, J. & Blumberg, W. E. Structural implications derived from the analysis of electron
291 paramagnetic resonance spectra of natural and artificial copper proteins. *Arch. Biochem. Biophys.*
292 **165**, 691-708 (1974)
- 293 19. Garajova, S. *et al.* Single-domain flavoenzymes trigger lytic polysaccharide monooxygenases for
294 oxidative degradation of cellulose. *Sci. Rep.* **6**, 28276 (2016)
- 295 20. Bennati-Granier, C. *et al.* Substrate specificity and regioselectivity of fungal AA9 lytic
296 polysaccharide monooxygenases secreted by *Podospora anserina*. *Biotechnol. Biofuels* **8**, 90 (2015)
- 297 21. Herpoël-Gimbert, I. *et al.* Comparative secretome analyses of two *Trichoderma reesei* RUT-C30 and
298 CL847 hypersecretory strains. *Biotechnol. Biofuels* **1**, 18 (2008)
- 299 22. Westereng, B. *et al.* Enzymatic cellulose oxidation is linked to lignin by long-range electron transfer.
300 *Sci. Rep.* **5**, 18561 (2015)
- 301 23. Villares, A. *et al.* Lytic polysaccharide monooxygenases disrupt the cellulose fibers structure. *Sci.*
302 *Rep.* **7**, 40262 (2017)

- 303 24. Frommhagen, M. *et al.* Discovery of the combined oxidative cleavage of plant xylan and cellulose by
304 a new fungal polysaccharide monooxygenase. *Biotechnol. Biofuels* **8**, 101 (2015)
- 305 25. Fanuel, M. *et al.* The *Podospora anserina* lytic polysaccharide monooxygenase PaLPMO9H
306 catalyzes oxidative cleavage of diverse plant cell wall matrix glycans. *Biotechnol. Biofuels* **10**, 63
307 (2017)
- 308 26. McCartney, L. *et al.* Differential recognition of plant cell walls by microbial xylan-specific
309 carbohydrate-binding modules. *Proc. Natl. Acad. Sci. U.S.A.* **103**, 4765-4770 (2006)
- 310 27. Nieduszynski, I. & Marchessault, R. H. Structure of beta-D-(1-->4')xylan hydrate. *Nature* **232**, 46-47
311 (1971)

312

313 **Figure legends**

314 **Figure 1. Phylogeny of the AA14 family of LPMOs.** Phylogenetic tree of 283 fungi analyzed
315 for AA14 members. The number of AA14 in fungal species (listed in **Supplementary Data Set**
316 **1**) is represented by red bars (the scale is indicated at the bottom of the figure). When available,
317 the mode of wood decay (brown-rots or white-rots) is specified next to the leaves of the tree.
318 Pictures illustrate the taxonomical diversity of wood-decaying fungi displaying AA14 LPMOs;
319 Genus (order) from top to bottom: *Xylaria* (Xylariales), *Trichoderma* (Hypocreales), *Nectria*
320 (Hypocreales), *Tremella* (Hypocreales), *Pycnoporus* (Polyporales), *Ganoderma* (Polyporales),
321 *Serpula* (Boletales), *Gymnopilus* (Agaricales). Photo credit: C. Lechat (AscoFrance) and A.
322 Favel (CIRM-CF).

323

324 **Figure 2. Structure of AA14 LPMO and organization of the copper active site.** (a) Overall
325 three-dimensional structure of *PcAA14B* (ribbon depiction with active site residues shown as
326 sticks under transparent surface). (b) Active site (Histidine brace) overlay of Cu-*LsAA9A*
327 (magenta) and *PcAA14B* (gold). (c) Continuous wave X-band EPR spectrum (9.3 GHz, 165 K)
328 with simulation (red) of *PcAA14A*. More data are presented in **Supplementary Figures 5** and **6**.

329

330 **Figure 3. Contribution of *PcAA14* enzymes to the saccharification of biomass.** (a) Glucose
331 release upon saccharification of pretreated pine and poplar by the CL847 *Trichoderma reesei*
332 enzyme cocktail in the presence of *PcAA14A* or *PcAA14B* and ascorbic acid. Glucose was
333 quantified using ionic chromatography. More saccharification assays are presented in
334 **Supplementary Figure 8**. (b) Dose effect of the addition of *PcAA14A* on the saccharification of

335 pretreated pine. Concentration of *PcAA14A* was 0.1 μM (+), 0.5 μM (++) and 1 μM (+++).
336 Error bars indicate standard error of the mean from triplicate independent experiments. Data
337 points are shown as dots.

338

339 **Figure 4. Enzymatic activity of *PcAA14* LPMOs.** (a) Morphology of birchwood cellulosic
340 fibers treated with *PcAA14A* and *PcAA14B* LPMOs. Images were recorded after dispersion.
341 Images are representative of the samples analyzed. (b) Solid state ^{13}C CP/MAS NMR analysis of
342 LPMO-treated cellulosic fibers. The differences in hemicellulose content in enzyme-treated
343 fibers were calculated from the C-1 and C-4 region deconvolution of NMR spectra and are
344 indicated in **Supplementary Figure 10**. (c) Assays in the presence of a GH11 xylanase were
345 performed on birchwood cellulose fibers. Xylobiose (X2) and xylotriose (X3) were quantified by
346 ionic chromatography. Error bars indicate standard error of the mean from triplicate independent
347 experiments. (d) Mass spectrometry identification of the X3 oxidized species detected at
348 429.13 m/z generated from birchwood cellulosic fibers by *PcAA14A* in synergy with a GH11
349 xylanase. The fragmentation pattern corresponds to a C1 oxidized species with an aldonic acid at
350 the reducing end. ∇ : water losses. \square : H_2CO losses. An expanded view of the spectrum is
351 provided in **Supplementary Figure 12**.

352

353 **On-line Materials and Methods**

354 **Transcriptomics and secretomics of *Pycnoporus* sp.**

355 Transcriptomic and proteomic data of three-days-old cultures of *Pycnoporus coccineus* BRFM
356 310 and *Pycnoporus sanguineus* BRFM 1264 grown on cellulose (Avicel), wheat straw, pine and
357 aspen are described in^{16,28}.

358 **Bioinformatic analysis of AA14 LPMOs**

359 *P. coccineus* AA14 sequences (Genbank ID KY769369 and KY769370) were compared to the
360 NCBI non redundant sequence database using BlastP²⁹ in February 2016. Blast searches
361 conducted with AA14 did not retrieve AA9s, AA10s, AA11s or AA13s with significant scores,
362 and vice-versa. MUSCLE³⁰ was used to perform multiple alignments. To avoid interference from
363 the presence or absence of additional residues, the signal peptides and C-terminal extensions
364 were removed. Bioinformatic analyses were performed on 286 fungal genomes sequenced and
365 shared by JGI collaborators. Protein clusters are available thanks to the JGI
366 (<https://goo.gl/ZAA2NX>) for each of these fungi. A phylogenetic tree has been inferred using 100
367 cleaned and merged alignments of proteins from selected clusters of proteins. Those clusters are
368 present, as much as possible, in all fungi in 1 copy in order to maximize the score $\sum 1/n$ (with n,
369 the number of copy in the genome). Sequences from clusters were aligned with Mafft³¹, trimmed
370 with Gblocks³² and a phylogenetic tree was built with concatenation of alignments with
371 Fasttree³³. The tree is displayed with Dendroscope³⁴ and Bio::phylo³⁵.

372 **Production of *P.coccineus* AA14 LPMOs**

373 The sequences corresponding to *PcAA14A* (Genbank ID KY769369) and *PcAA14B* (Genbank ID
374 KY769370) genes from *P. coccineus* BRFM310 were synthesized after codon optimization for

375 expression in *P. pastoris* (GenScript, Piscataway, USA). The region corresponding to the native
376 signal sequence was kept while the C-terminal extension region was removed. Synthesized genes
377 were further inserted with into a modified pPICZ α A vector (Invitrogen, Cergy-Pontoise, France)
378 using *Bst*BI and *Xba*I restriction sites in frame with the (His)₆-tag located at the C-terminus of
379 recombinant proteins. Fusion of *PcAA14A* with CBM1 was carried using the CBM1 domain of
380 *PaLPMO9E*, which was added to *PcAA14A* at the end of the catalytic module using the linker
381 sequence of *PaLPMO9E*²⁰. Constructs without (His)₆-tag sequence were also designed by adding
382 a stop codon at the end of the AA14 catalytic module. *P. pastoris* strain X33 and the pPICZ α A
383 vector are components of the *P. pastoris* Easy Select Expression System (Invitrogen), all media
384 and protocols are described in the manufacturer's manual (Invitrogen).

385 Transformation of competent *P. pastoris* X33 was performed by electroporation with *Pme*I-
386 linearized pPICZ α A recombinant plasmids and zeocin-resistant *P. pastoris* transformants were
387 screened for protein production as described in³⁶. The best-producing transformants were grown
388 in 2 L of BMGY medium containing 1 mL.L⁻¹ *Pichia* trace minerals 4 (PTM₄) salts in shaken
389 flasks at 30°C in an orbital shaker (200 rpm) to an OD₆₀₀ of 2 to 6. Cells were then transferred to
390 400 mL of BMMY medium containing 1 mL.L⁻¹ of PTM₄ salts at 20°C in an orbital shaker (200
391 rpm) for 3 days, with supplementation of 3% (v/v) methanol every day.

392 Bioreactor productions were carried out in 1.3-L New Brunswick BioFlo[®] 115 fermentors
393 (Eppendorf, Hamburg, Germany) following the *P. pastoris* fermentation process guidelines
394 (Invitrogen). Recombinant enzymes were secreted up to ~1 g.L⁻¹ (**Supplementary Figure 13**).

395 **Purification of *PcAA14* LPMOs**

396 The culture supernatants were recovered by pelleting the cells by centrifugation at 2,700 g for
397 5 min, 4°C and filtered on 0.45 µm filters (Millipore, Molsheim, France). For (His)₆-tagged
398 enzymes, the pH was adjusted to 7.8 and the supernatants were loaded onto 5 ml His Trap HP
399 columns (GE healthcare, Buc, France) connected to an Akta Xpress system (GE healthcare).
400 Prior to loading, the columns were equilibrated in 50 mM Tris HCl pH 7.8; 150 mM NaCl
401 (buffer A). The loaded columns were then washed with 5 column volumes (CV) of 10 mM
402 imidazole in buffer A, before the elution step with 5 CV of 150 mM imidazole in buffer A.
403 Fractions containing the protein were pooled and concentrated with a 3-kDa vivaspin
404 concentrator (Sartorius, Palaiseau, France) before loading onto a HiLoad 16/600 Superdex 75
405 Prep Grade column (GE Helthcare) and separated in 50 mM sodium acetate buffer pH 5.2. Gel
406 filtration analysis showed that both *PcAA14* proteins are monomeric in solution. For enzymes
407 without (His)₆-tag, salts contained in the culture media were diluted ten-fold in 20 mM Tris-HCl
408 pH 8, then culture supernatants were concentrated with a Pellicon-2 10-kDa cutoff cassette
409 (Millipore) to a volume of approx. 200 mL and loaded onto a 20-mL High Prep DEAE column
410 (GE Helthcare). Proteins were eluted using a linear gradient of 1 M NaCl (0 to 700 mM in 200
411 mL). Fractions were then analyzed by SDS PAGE and those containing the recombinant protein
412 were pooled and concentrated. The concentrated proteins were then incubated with one-fold
413 molar equivalent of CuSO₄ overnight before separation on a HiLoad 16/600 Superdex 75 Prep
414 Grade column in 50 mM sodium acetate buffer pH 5.2.

415 **Biochemical analysis of AA14 LPMOs**

416 Concentration of purified proteins was determined by using the Bradford assay (Bio-Rad,
417 Marnes-la-Coquette, France) or using a nanodrop ND-2000 device with calculated molecular
418 mass and molar extinction coefficients derived from the sequences. Proteins were loaded onto

419 10% SDS-PAGE gels (Thermo Fisher Scientific, IL, USA) which were stained with Coomassie
420 Blue. The molecular mass under denaturing conditions was determined with reference standard
421 proteins (Page Ruler Prestained Protein Ladder, Thermo Fisher Scientific). Native IEF was
422 carried out in the Bio-Rad gel system, using pI standards ranging from 4.45 to 8.2 (Bio-Rad).

423 **N-terminal amino acid sequence determination**

424 The N-terminal amino acid sequences of purified *PcAA14A* and *PcAA14B* were determined
425 according to the Edman degradation. Samples were electroblotted onto a polyvinylidene
426 difluoride membrane (iBlot, Life Technologies). Analyses were carried out on a Procise
427 Sequencing System (ThermoFisher).

428 **Matrix-assisted laser desorption ionization/mass spectrometry**

429 Matrix-assisted laser desorption ionization mass spectra analyses were performed on a Microflex
430 II mass spectrometer (Bruker Daltonics). One μL of matrix [10 mg of 2,5-dihydroxybenzoic acid
431 in 1 mL of $\text{CH}_3\text{CN}/\text{H}_2\text{O}$ 50/50 (v/v), 0.1% formic acid (v/v)] was added to 1 μL of intact
432 *PcAA14A* or *PcAA14B* protein sample (100 pmoles) in the same solution. Then, mixtures were
433 allowed to dry at room temperature. Data acquisition was operated using the Flex control
434 software. External mass calibration was carried out on Peptide calibration standard (Bruker
435 Daltonics).

436 **Deglycosylation assays**

437 To remove N-linked glycans, purified enzymes were treated with EndoHf (New England
438 Biolabs, Ipswich, MA) under denaturing conditions according to the manufacturer's instructions.
439 Briefly, 10 μg of protein were incubated in 0.5% SDS and 40 mM DTT and heated for 10 min at
440 100°C for complete denaturation. Denaturated samples were subsequently incubated with 1,500

441 units of EndoHf in 50 mM sodium acetate pH 6.0 for 1 h at 37°C. Deglycosylated and control
442 samples were analyzed by SDS-PAGE.

443 **Amplex Red assay**

444 A fluorimetric assay based on Amplex Red and horseradish peroxidase was used as described
445 previously³⁷. The reaction (total volume 100 μ L, 30°C, 30 min) was measured in 50 mM sodium
446 acetate buffer pH 6.0 containing 50 μ M Amplex Red (Sigma-Aldrich, Saint-Quentin Fallavier,
447 France), 7.1 U.mL⁻¹ horseradish peroxidase, 0.2 to 4 μ M enzyme, and 50 μ M reductant, i.e.
448 ascorbate, *p*-coumaric acid, caffeic acid, cinapic acid, vanillic acid, menadione, L-cysteine,
449 tannic acid, syringic acid, gallic acid, 3-hydroxyanthranilic acid (3-HAA) and epigallocatechin
450 gallate in water and fluorescence was detected using an excitation wavelength of 560 nm and an
451 emission wavelength of 595 nm using a Tecan Infinite M200 plate reader (Tecan, Männedorf,
452 Switzerland). The specific activity was counted from H₂O₂ calibration curve, and the slope
453 (13,227 counts. μ mol⁻¹) was used to convert the fluorimeters' readout (counts.min⁻¹) into enzyme
454 activity.

455 **ICP/MS Analysis**

456 To obtain apo enzymes, 100 mM EDTA treatment was performed overnight. Prior to the
457 analysis, samples were mineralized in a mixture containing 2/3 of nitric acid (Sigma-Aldrich,
458 65% Purissime) and 1/3 of hydrochloric acid (Fluka, 37%, Trace Select) at 120°C. The residues
459 were diluted in ultra-pure water (2 mL) before ICP/MS analysis. The ICP-MS instrument was an
460 ICAP Q (ThermoElectron, Les Ullis, France), equipped with a collision cell. The calibration
461 curve was obtained by dilution of a certified multi-element solution (Sigma-Aldrich). Copper

462 concentrations were determined using Plasmalab software (Thermo-Electron), at a mass of
463 interest $m/z=63$.

464 **Saccharification assays**

465 Wheat straw, pine and poplar biomass were pretreated under acidic conditions. Sugar
466 composition was determined using the alditol acetate method.³⁸ Wheat straw consisted of 51.98
467 ± 2.02 % (w/v) glucose, 5.70 ± 0.23 % (w/v) xylose and 0.46 ± 0.04 % (w/v) arabinose. Pine
468 consisted of 43.25 ± 1.34 % (w/v) glucose, 0.24 ± 0.01 % (w/v) xylose and 0.15 ± 0.02 % (w/v)
469 arabinose. Poplar consisted of 50.85 ± 0.91 % (w/v) glucose, 0.39 ± 0.01 % (w/v) xylose and
470 0.07 ± 0.01 % (w/v) arabinose. The enzymatic treatments were carried out in sodium acetate
471 buffer (50 mM, pH 5.2) in a final volume of 1 ml at 0.5% consistency (w d.m./v). The LPMO
472 treatment was carried out sequentially with a CL847 *T. reesei* enzyme cocktail²¹ provided by
473 IFPEN (Rueil-Malmaison, France). Each *PcAA14* enzyme was added to the substrate at a
474 concentration of between 0.1 and 1 μ M in the presence or absence of 1 mM ascorbic acid for
475 72 h, followed by addition of 1 $\text{mg}\cdot\text{g}^{-1}$ dry matter (d. m.) substrate of commercial cellulases from
476 *T. reesei* for 24 h. Enzymatic treatments were performed in 2-ml tubes incubated at 45°C and
477 850 rpm in a rotary shaker (Infors AG, Switzerland). Then, samples were centrifuged at 14,000 *g*
478 for 5 min at 4°C and the soluble fraction was heated for 10 min at 100°C to stop the enzymatic
479 reaction. Glucose was quantified by high performance anion exchange chromatography coupled
480 with amperometric detection (HPAEC-PAD) as described in²⁰.

481 **Polysaccharides cleavage assays**

482 Avicel was purchased from Sigma-Aldrich and lichenan (from Icelandic moss), curdlan, starch,
483 barley β -1,3/1,4-glucan, konjac glucomannan, wheat arabinoxylan, tamarind xyloglucan were

484 purchased from Megazyme (Wicklow, Ireland). PASC was prepared from Avicel as described
485 previously²⁰ in 50 mM sodium acetate buffer pH 5.2. A similar protocol was used to prepare
486 swollen squid pen chitin provided by Dominique Gillet (Mahtani Chitosan, India).
487 Glucuronoxylans were extracted from birchwood as described previously³⁹.

488 All the cleavage assays contained between 0.5 and 1 μ M of *PcAA14s* in the presence of 1 mM
489 ascorbate and 0.1% (w/v) polysaccharides. The enzyme reactions were performed in 2-mL tubes
490 and incubated in a thermomixer (Eppendorf, Montesson, France) at 45°C and 850 rpm. After 16
491 h of incubation, samples were heated for 10 min at 100°C to stop the enzymatic reaction and then
492 centrifuged at 14,000 *g* for 15 min at 4°C to separate the soluble fraction from the remaining
493 insoluble fraction before determination of soluble products using HPAEC as described above
494 with oligosaccharides standards (Megazyme).

495 **Microscopy**

496 Aqueous dispersions of Kraft birchwood cellulosic fibers (kindly provided by Sandra Tapin,
497 FCBA, Grenoble, France) were adjusted to pH 5.2 with acetate buffer (50 mM) in a final
498 reaction volume of 5 mL. Each *PcAA14* enzyme was added to the fibers at a final concentration
499 of 20 mg.g⁻¹ in the presence of 1 mM of ascorbic acid. Enzymatic incubation was performed at
500 40 °C under mild agitation for 48 h. Samples were then dispersed by a Polytron PT 2100
501 homogenizer (Kinematica AG, Germany) for 3 min, and ultrasonicated by means of a QSonica
502 Q700 sonicator (20 kHz, QSonica LLC., Newtown, USA) at 350 W ultrasound power for 3 min
503 as described previously²³. The reference sample was submitted to the same treatment but it did
504 not contain the *PcAA14* enzyme. Birchwood cellulose fibers (reference and *PcAA14*-treated)
505 were deposited onto a glass slide and observed by a BX51 polarizing microscope (Olympus
506 France S.A.S.) with a 4 \times objective. Images were captured by a U-CMAD3 camera (Olympus

507 Japan). For the atomic force microscopy (AFM) experiments, samples were deposited onto mica
508 substrates from fiber solutions at 0.1 g L^{-1} , and allowed to dry overnight. Topographical images
509 on mica were registered by a Nanoscope III-A AFM (Bruker, Santa Barbara, US). The
510 images were collected in tapping mode under ambient air conditions (temperature and relative
511 humidity) using a monolithic silicon tip (RFESP, Bruker) with a spring constant of 3 N m^{-1} ,
512 and a nominal frequency of 75 kHz . Image processing was performed with the WSxM 5.0
513 software. For transmission electron microscopy (TEM) experiments, fiber solutions at 0.1 g L^{-1}
514 in water were deposited on freshly glow-discharged carbon-coated electron microscope grids
515 (200 mesh, Delta Microscopies, France) and the excess of water was removed by blotting. The
516 sample was then immediately negatively stained with uranyl acetate solution (2%, w/v) for 2 min
517 and dried after blotting. The grids were observed with a Jeol JEM 1230 TEM at 80 kV .

518 **NMR spectroscopy**

519 Solid state ^{13}C NMR experiments were performed on a Bruker Avance III 400 spectrometer
520 operating at a ^{13}C frequency of 100.62 MHz using a 4 mm double-resonance (H/X) magic angle
521 spinning (MAS) probe. Samples were dialyzed against ultrapure water (MWCO 12-14000) for 7
522 days to remove buffer, ascorbate and released soluble sugars. Experiments were conducted at
523 room temperature at a MAS frequency of 9 kHz using a cross-polarization sequence (CP/MAS).
524 The ^{13}C chemical shift was referenced using the carbonyl signal of glycine at 176.03 ppm . The
525 cross polarization pulse sequence parameters were: $3.2 \mu\text{s}$ proton 90° pulse, 2.50 ms contact time
526 at 67.5 kHz , and 10 s recycle time. Typically, the accumulation of $5,120$ scans was used. All
527 spectra obtained were processed and analyzed using Bruker Topspin version 3.2. To determine
528 the crystallinity and the general cellulose's morphology of the C-1 and C-4 region of the
529 samples, we used the sophisticated approach⁴⁰ that is described in details in our previous work²³.

530 For the C1-region, this approach used three Lorentzian lines for the crystalline part (Cr (I α) and
531 Cr (I β)) and one Gaussian line for the less ordered cellulose (para-crystalline cellulose, PCr). For
532 the C-4 region, four lines for the crystalline part corresponding to crystalline and para-crystalline
533 (PCr) cellulose and three Gaussian lines for the amorphous part (accessible surfaces, AS, and
534 inaccessible surface, IAS) were used. The cellulosic fibers contained xylan, which was
535 considered in the spectral decomposition: in the C-1 region with one line at 101.4 ppm and in the
536 C-4 region with one broad line centered at 81.6 ppm.

537 **Synergy assays with xylanase**

538 Assays were run on the birchwood cellulose fibers used in microscopy and NMR experiments.
539 Fibers were grinded (< 0.18 mm particle size) and hydrated in water under stirring for 48 h prior
540 to enzymatic assays. One mL reaction volumes containing 0.5% (w/v) birchwood fibers were
541 incubated with 1 μ M of PcAA14s and 0.1 μ M of GH11 xylanase M4 (*Aspergillus niger*) from
542 Megazyme (reference E-XYAN4) in 10 mM sodium acetate pH 5.2 supplemented or not with
543 1 mM L-cysteine. Prior to the reaction, the GH11 xylanase was buffer exchanged with 10 mM
544 sodium acetate pH 5.2 using a PD-10 column (GE Helthcare) to remove any trace of ammonium
545 sulfate. Enzymatic reactions were performed in 2-mL tubes and incubated in a thermomixer
546 (Eppendorf, Montesson, France) at 45°C and 850 rpm for 24 h. Samples were then centrifuged at
547 14,000 g for 5 min at 4°C to separate the soluble fraction from the remaining insoluble fraction.
548 Proteins were removed from the soluble oligosaccharides fraction by filtering the supernatants
549 using Nanosep 3K Omega centrifugal devices (Pall corporation). Soluble oligosaccharides
550 generated were analyzed by HPAEC as described previously and mass spectrometry (see below)
551 using non-oxidized xylo-oligosaccharides (Megazyme) as standards. Corresponding C1-oxidized

552 standards (from DP2 to DP4) were produced from non-oxidized xylo-oligosaccharides by using
553 purified *Pa*CDHB prepared as described previously.²⁰ All assays were carried out in triplicate.

554 **Electrospray mass spectrometry (ESI-MS and MS/MS)**

555 Experiments were performed on a Synapt G2Si high-definition mass spectrometer (Waters
556 Corp., Manchester, UK) equipped with an Electrospray ion (ESI) source. Two types of mass
557 measurements were performed on the samples: firstly, a mass profile was done on a mass range
558 of 300-2000 m/z (M/S). Ions of interest were further isolated and fragmented by collision-
559 induced dissociation in the transfer cell of the instrument (MS/MS). In these experiments, ion
560 mobility (IM) was activated to reduce interference from sample impurities. IM was performed in
561 a travelling-wave ion mobility (TWIM) cell. The gas flows were held at 180 $\text{mL}\cdot\text{min}^{-1}$ He in the
562 helium cell and at 90 $\text{mL}\cdot\text{min}^{-1}$ N_2 in the mobility cell. The IM traveling wave height was set to
563 40 V and its wave velocity was set to 480 $\text{m}\cdot\text{s}^{-1}$ for positive ionization mode and 500 $\text{m}\cdot\text{s}^{-1}$ for
564 negative ionization mode. Samples were diluted 10-fold in MeOH/ H_2O (1:1, v/v) and infused at
565 a flow rate of 5 $\mu\text{L}\cdot\text{min}^{-1}$ in the instrument. The instrument was operated in positive or negative
566 polarity, and in “sensitivity” mode.

567 **Crystallization, data collection, structure determination and refinement**

568 All crystallization experiments were carried out at 20°C by the sitting-drop vapour-diffusion
569 method using 96-well crystallization plates (Swissci) and a Mosquito[®] Crystal (TTP labtech)
570 crystallization robot. Reservoirs consisted of 40 μL of commercial screens and crystallization
571 drops were prepared by mixing 100 nL reservoir solution with 100, 200 and 300 nL of protein
572 solution. An initial hit was obtained after 1 week from a condition of the AmSO₄ screen (Qiagen)
573 consisting of 2.4 M $(\text{NH}_4)_2\text{SO}_4$ and 0.1 M citric acid pH 4.0. This condition was further

574 optimized to obtain diffraction-grade crystals by mixing protein solution at 28 mg mL⁻¹ with
575 precipitant solution consisting of 2.4 M (NH₄)₂SO₄ and 0.1 M citric acid pH 4.4 at a volume ratio
576 of 3:1. *PcAA14B* crystals grew to dimensions of 0.15×0.15×0.05 mm in one week. Crystals
577 belong to space group P4₁2₁2 with cell axes 204×204×110 Å and two molecules *per* asymmetric
578 unit.

579 Crystals of *PcAA14B* were soaked for 5 min in a solution where 2.4 M (NH₄)₂SO₄ of the mother
580 liquor was replaced by 2.4 M Li₂SO₄ for the sake of cryoprotection prior to flash-cooling in
581 liquid nitrogen. As X-ray fluorescence scans on native crystals did not reveal a significant
582 presence of copper within the crystals, a heavy atom derivative was prepared by soaking the
583 crystals in reservoir solution supplemented with 55 mM of the gadolinium complex gadoteridol
584 prior to cryo-cooling. Native diffraction data were collected on beamline ID23-1, while a MAD
585 dataset at wavelengths of 1.711 and 1.698 Å for peak/inflection and remote energies, was
586 collected on beamline ID30B at the European Synchrotron Radiation Facility (ESRF), Grenoble,
587 France. Data were indexed and integrated in space group P4₁2₁2 using XDS⁴¹ and subsequent
588 processing steps were performed with the CCP4 software suite⁴². Determination of the Gd³⁺
589 substructure and subsequent phasing combined with solvent flattening were carried out with
590 SHELXC/D/E⁴², leading to a pseudo-free correlation coefficient of 71.8%. Starting from
591 experimental phases, an initial model comprising 526 residues (out of 584), was automatically
592 built with Buccaneer⁴³ and manually completed with Coot⁴⁴. This initial model was used for
593 rigid body refinement followed by restrained refinement against native data with the program
594 Refmac⁴⁵. A random set of 5% of reflections was set aside for cross-validation purposes. Model
595 quality was assessed with internal modules of Coot⁴⁴ and using the Molprobity server⁴⁶. Figures
596 representing structural renderings were generated with the PyMOL Molecular Graphics System

597 (DeLano, W.L. The PyMOL Molecular Graphics on <http://www.pymol.org/>). Atomic
598 coordinates and structure factors have been deposited within the Protein Data Bank
599 <http://www.rcsb.org>⁴⁷. Data collection and refinement statistics are summarized in
600 **Supplementary Table 4.**

601 **EPR**

602 Continuous wave (cw) X-band frozen solution EPR spectra of a 0.2 to 0.3 mM solution of
603 Cu(II)-*PcAA14A* and *PcAA14B*, prepared and copper loaded as described above, in 10% v/v
604 glycerol at pH 5.2 (50 mM sodium acetate buffer) and 165 K were acquired on a Bruker EMX
605 spectrometer operating at ~9.30 GHz, with modulation amplitude of 4 G, modulation frequency
606 100 kHz and microwave power of 10.02 mW (4 scans). Both enzymes showed identical EPR
607 spectra. Cw Q-band frozen solution spectra of 1.0 mM solution of Cu(II)- *PcAA14A* at pH 5.2
608 (50 mM sodium acetate buffer) and 113 K were acquired on a Jeol JES-X320 spectrometer
609 operating at ~34.7 GHz, with modulation width 1 mT and microwave power of 1.0 mW (8
610 scans).

611 Spectral simulations were carried out using EasySpin 5.0.3⁴⁸. Simulation parameters are given in
612 **Supplementary Table 3.** g_z and $|A_z|$ values were determined accurately from the absorptions at
613 low field. It was assumed that g and A tensors were axially coincident. Accurate determination
614 of the g_x , g_y , $|A_x|$ and $|A_y|$ was obtained by simultaneous fitting of both X and Q band spectra.
615 The superhyperfine coupling values for the nitrogen atoms could not be determined accurately,
616 although it was noted that satisfactory simulation could only be achieved with the addition of
617 two nitrogen atoms with coupling in the range 30-36 MHz.

618 **Statistics**

619 For all statistics, $n = 3$ values were used to calculate the standard error of the mean. Values
620 resulted from independent experiments. For all representative results, experiments were repeated
621 at least two times and at least 20 images were collected for microscopy analyses.

622

623 **Accession codes**

624 *PcAA14A* and *PcAA14B* sequences were deposited in GenBank under accession numbers
625 KY769369 and KY769370, respectively. The X-ray structure of *PcAA14B* was deposited in the
626 Protein Data Bank with accession 5NO7. Raw EPR data are available on request through the
627 Research Data York (DOI: 10.15124/8758d712-1e67-467e-b0f0-f0dd99f0232a).

628 **Data Availability Statement**

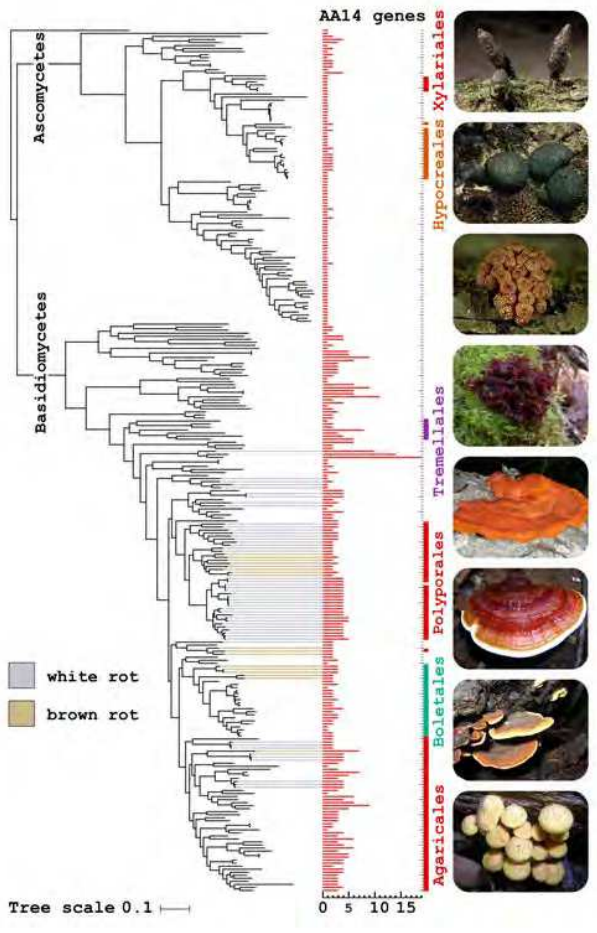
629 All data generated or analysed during this study are included in this published article (and its
630 supplementary information files).

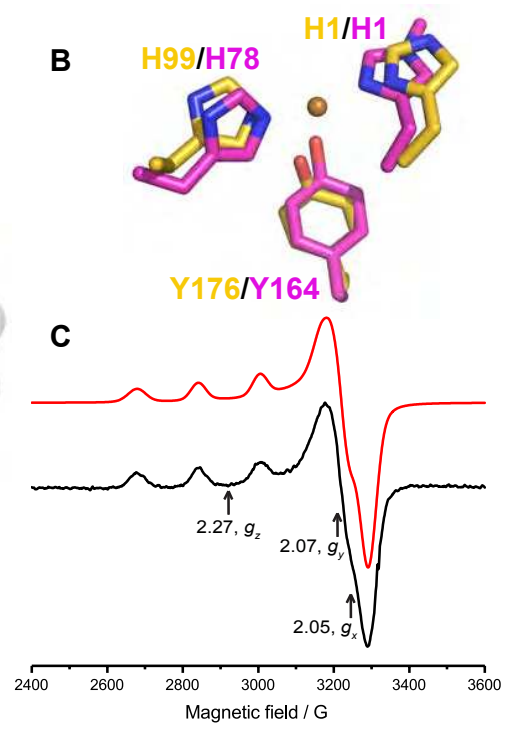
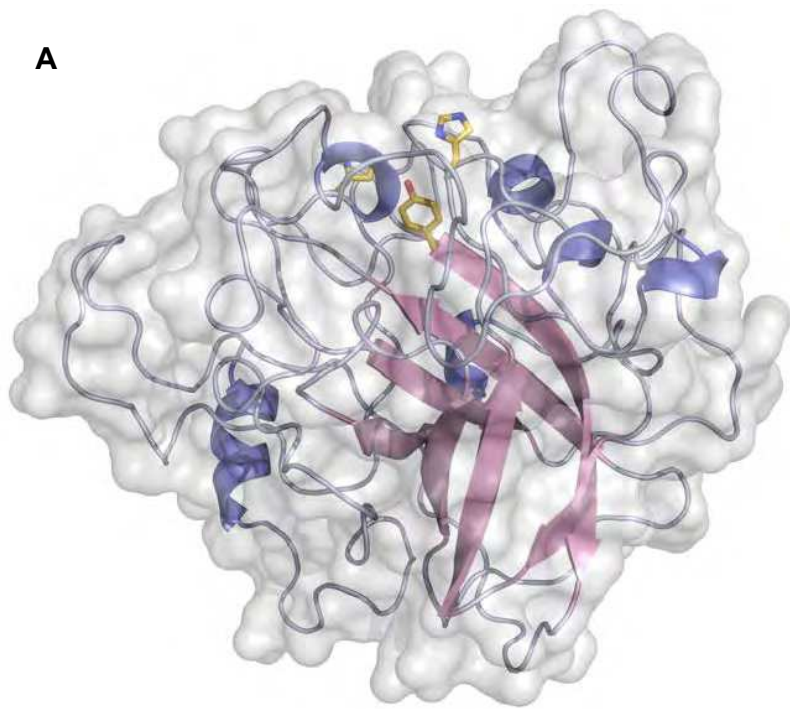
631

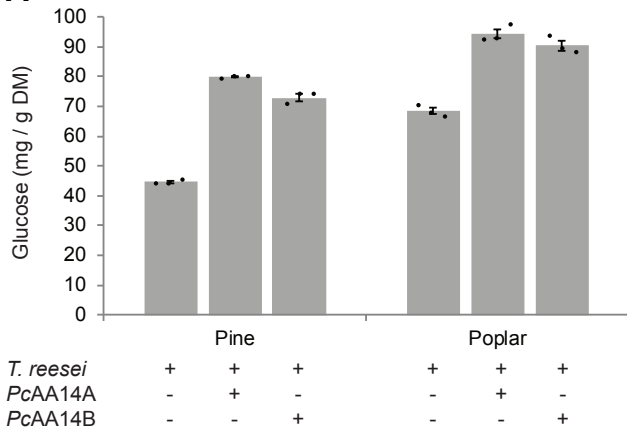
632 **Methods-only references**

- 633 28. Miyauchi, S. *et al.* Visual Comparative Omics of Fungi for Plant Biomass Deconstruction.
634 *Front. Microbiol.* **7**, 1335 (2016)
- 635 29. Altschul, S. F., Gish, W., Miller, W., Myers, E. W. & Lipman, D. J. Basic local alignment
636 search tool. *J. Mol. Biol.* **215**, 403-410 (1990)
- 637 30. Edgar, R. C. MUSCLE: multiple sequence alignment with high accuracy and high
638 throughput. *Nucleic Acids Res.* **32**, 1792-1797 (2004)
- 639 31. Katoh, K. & Standley, D. M. MAFFT multiple sequence alignment software version 7:
640 improvements in performance and usability. *Mol. Biol. Evol.* **30**, 772-780. (2013)
- 641 32. Talavera, G. & Castresana, J. Improvement of phylogenies after removing divergent and
642 ambiguously aligned blocks from protein sequence alignments. *Syst. Biol.* **56**, 564-577
643 (2007)
- 644 33. Price, M. N., Dehal, P. S. & Arkin, A. P. FastTree 2--approximately maximum-likelihood
645 trees for large alignments. *PLoS One* **5**, e9490 (2010)

- 646 34. Huson, D. H. & Scornavacca, C. Dendroscope 3: an interactive tool for rooted phylogenetic
647 trees and networks. *Syst. Biol.* **61**, 1061-1067 (2012)
- 648 35. Vos, R. A., Caravas, J., Hartmann, K., Jensen, M.A. & Miller, C. BIO:Phylo-
649 phyloinformatic analysis using perl. *BMC Bioinformatics* **12**, 632011 (2011)
- 650 36. Haon, M. *et al.* Recombinant protein production facility for fungal biomass-degrading
651 enzymes using the yeast *Pichia pastoris*. *Front. Microbiol.* **6**, 1002 (2015)
- 652 37. Kittl, R., Kracher, D., Burgstaller, D., Haltrich, D. & Ludwig, R. Production of four
653 *Neurospora crassa* lytic polysaccharide monooxygenases in *Pichia pastoris* monitored by a
654 fluorimetric assay. *Biotechnol. Biofuels* **5**, 79 (2012)
- 655 38. Englyst, H.N. & Cummings, J.H. Improved method for measurement of dietary fiber as non-
656 starch polysaccharides in plant foods. *J. Assoc. Off. Anal. Chem.* **71**, 808-814 (1988)
- 657 39. Westbye, P., Svanberg, C. & Gatenholm, P. The effect of molecular composition of xylan
658 extracted from birch on its assembly onto bleached softwood kraft pulp. *Holzforschung* **60**,
659 143-148 (2006)
- 660 40. Larsson, P. T., Wickholm, K. & Iversen, T. A CP/MAS ¹³C NMR investigation of molecular
661 ordering in celluloses. *Carbohydrate Research* **302**, 19-25 (1997)
- 662 41. Kabsch, W. XDS. *Acta Crystallogr. D Biol. Crystallogr.* **66**, 125-132 (2010)
- 663 42. Winn, M. D. *et al.* Overview of the CCP4 suite and current developments. *Acta Crystallogr.*
664 *D Biol. Crystallogr.* **67**, 235-242 (2011)
- 665 43. Cowtan, K. The Buccaneer software for automated model building. 1. Tracing protein
666 chains. *Acta Crystallogr. D Biol. Crystallogr.* **62**, 1002-1011 (2006)
- 667 44. Emsley, P., Lohkamp, B., Scott, W. G. & Cowtan, K. Features and development of Coot.
668 *Acta Crystallogr. D Biol. Crystallogr.* **66**, 486-501 (2010)
- 669 45. Murshudov, G. N., Vagin, A. A. & Dodson, E. J. Refinement of macromolecular structures
670 by the maximum-likelihood method. *Acta Crystallogr. D Biol. Crystallogr.* **53**, 240-255
671 (1997)
- 672 46. Chen, V. B. *et al.* MolProbity: all-atom structure validation for macromolecular
673 crystallography. *Acta Crystallogr. D Biol. Crystallogr.* **66**, 12-21 (2010)
- 674 47. Berman, H., Henrick, K. & Nakamura, H. Announcing the worldwide Protein Data Bank.
675 *Nat. Struct. Biol.* **10**, 980 (2003)
- 676 48. Stoll, S. & Schweiger, A. EasySpin, a comprehensive software package for spectral
677 simulation and analysis in EPR. *J. Magn. Reson.* **178**, 42-55 (2006)
- 678





A**B**